Connecting earthquake triggering to dynamic strain

Nicholas J. van der Elst and Emily E. Brodsky

Dept. of Earth and Planetary Science, University of California, Santa Cruz

nvanderelst@es.ucsc.edu

1) Dynamic strains trigger earthquakes.

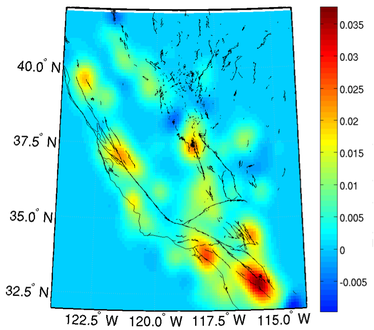

Fig 1a. Triggering in California is ubiquitous (left). Geothermal areas are highlighted, but triggering occurs in all seismically active regions (below).

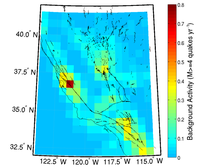

Fig 1b. Background activity from Hardebeck et al., 2008.

The sensitivity of faults to dynamic triggering reveals information about the mechanics of earthquake nucleation. Here we use a new statistical metric to examine the scaling of earthquake triggering with the amplitude of the triggering strain in the near and farfield in two tectonically distinct regions: California and Japan.

Methods - Measuring Triggering Intensity

Compare the waiting time to the first post-trigger earthquake to the time since the last local earthquake.

$$R = \frac{t_2}{t_1 + t_2} \quad (1)$$

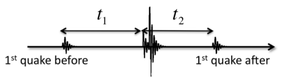

If triggering is absent, R is uniformly distributed between 0 and 1 for a population of earthquakes. A high proportion of R's<0.5 indicates triggering.

Triggering intensity is calculated from the mean of R using a statistical model of earthquake occurence times. For a step change in a Poisson process, for example, the expectation of R is

$$< R >= \frac{1}{n^2}\left((n+1)\ln(n+1) - n\right) \quad (2)$$

$$n = \frac{\lambda_2 - \lambda_1}{\lambda_1} \quad (3)$$

where λ_i are the average earthquake rates before and after the trigger. From the observed mean of R we solve for triggering intensity n.

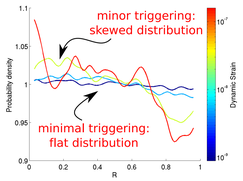

Fig 2a. Distribution of R values for **long-range triggers > 800 km**.

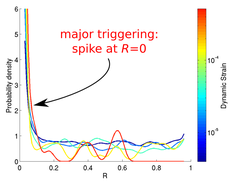

Fig 2b. Distribution of R values for **short-range triggers < 6 km from mainshock**

2) Triggering intensity scales with dynamic strain.

We know that farfield triggering is caused by dynamic strain (seismic waves). We expect dynamic strain to also trigger earthquakes in the nearfield, although the relative importance of dynamic vs. static triggering mechanisms may decrease in the nearfield. If we project the proportionality determined in the farfield into the near field, we should see any additional nearfield triggering component as a superposition on top of the projected relationship.

We find that **triggering intensity scales with dynamic strain** and that the proportionality is identical in both the near and farfield. **No additional near field component is required** to explain the data. We also find that triggerability varies geographically and **Japan is less triggerable than California.**

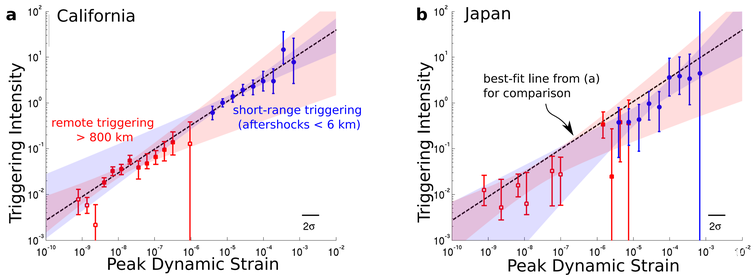

Fig 3. Triggering intensity (eq. 3) as a function of peak dynamic strain for two separate datasets. (a) Triggering in California. (b) Triggering in Japan. Error bars are 95% confidence limits from 1000 bootstrap resamplings. Dashed line is the best fit to the California data, plotted in both panels for easy comparison. Confidence bounds (95%) for separate linear regressions of the long and short-range data are shaded red and blue, respectively. Japan is less triggerable than California. Note that for Japan, where the short and long-range data overlap, triggering rates are identical.

Estimating strain: empirical ground motion regressions

Long-range triggers

Dynamic strain is estimated for distant triggers with the surface wave magnitude equation:

$$\log A = M_S - 1.66 \log \Delta - 2 \quad (4)$$

where, A is displacement in micrometers and Δ is in degrees.

Short-range triggers

Dynamic strain from short-range triggers (local mainshocks) is determined from a ShakeMap regression (Boatwright, 2003).

$$\log V = 1.06 M_L - 0.0063 r - \log r + 1.35 \quad (5)$$

Peak dynamic strain

Strains are then estimated as displacement over wavelength, or particle velocity over phase velocity.

$$\epsilon = \frac{A}{\lambda} = \frac{V}{c_s} \quad (6)$$

References:

Felzer, K. R., and E. E. Brodsky (2005), Testing the stress shadow hypothesis, *J. Geophys. Res.* 110 (B5), 13.

Boatwright, J., H. Bundock, J. Luetgert et al. (2003), The Dependence of PGA and PGV on Distance and Magnitude Inferred from Northern California ShakeMap Data, *Bull. Seismo. Soc. Amer.* 93 (5), 2043.

Hardebeck, J. L., K. R. Felzer, A. J. Michael (2008), Improved tests reveal that the accelerating moment release hypothesis is statistically insignificant, J. *Geophys. Res. 113*.

3) The threshold for triggering in Californai is < 3e-9 strain.

\We can express triggering intensity n (eq 3) in terms of the probability of seeing a triggered earthquake in its own recurrence interval. For a step change in the intensity of a Poisson process,

$$P(N_{EQ} > 0 \mid n) = 1 - exp\{-(n+1)\} \quad (7).$$

The threshold for observable triggering in California is 3e-9 strain, orders of magnitude lower than previously estimated. By looking at the statistics of entire populations of earthquakes and not identifiying any specific earthquake as triggered or not, the method can identify this small triggering signal.

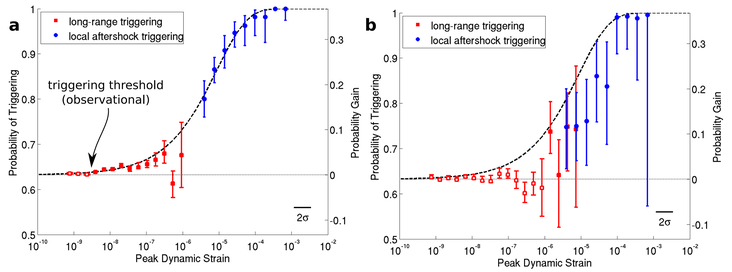

Fig 4. Probability of seeing a triggered earthquake (eq. 7) as a function of peak dynamic strain. (a) California. (b) Japan. Long-range (>800 km) triggers are in red and short-range triggers (local aftershocks <6 km) are in blue. Error bars are 95% confidence limits from 1000 bootstrap resamplings.

Validation and calibration: ETAS simulations

In calculating triggering intensity, we assumed 1) an exponential (Poisson-type) distribution of interevent times, and 2) that R is calculated only for causally related earthquakes. In practice, however, we simply use the first earthquake before and after a potential trigger. These earthquake pairs are sometimes unconnected, and introduce uniformly-distributed "noise" into the R distribution. To examine the effect of this simplification, we run statistical simulations using a modified ETAS model, and compare to the observations.

ETAS model

The ETAS model uses empirical descriptions of earthquake clustering in space and time to generate realistic earthquake catalogs:

1) Magnitudes are drawn from the Gutenberg-Richter distribution.
2) Omori's law governs decay of triggering with time.
3) A spatial kernel describes the decay of aftershock triggering with distance from the parent quake.
4) A productivity law describes how the number of triggered aftershocks scales with mainshock magnitude.

Modified model

We replace rule 3 and 4 with the rule that triggering is directly proportional to strain (peak ground motion) from Eqs. 4 and 5. This constitutes an **earthquake clustering model based on observed ground motions**.

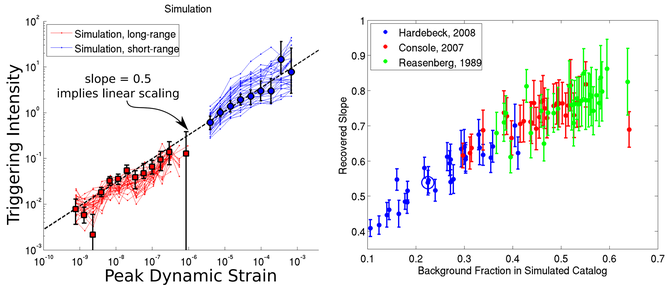

Fig 5. The R-statistic applied to simulated (modified ETAS) seismicity catalogs (thin lines). (**a**) The rule that triggering is directly proportional to strain reproduces the observations. The filled symbols are the real data for California from fig. 3 and agree well with the simulation results. (**b**) The recovered slope scales with background fraction in the catalog. Different colors represent simulations using different estimates of the bulk short-range triggering statistics taken from the literature. This implies that the background fraction in the California catalog is on the order of 20-30%.

The constant of proportionality is set to agree with bulk aftershock statistics for California from Hardebeck, et al. (2008). This allows us to simulate triggering from large distant earthquakes as well as local aftershocks. Note that the long-range triggering component of the simulation is tuned only based on short-range aftershock productivity.

Results

Applying the R statistic to the simulated catalog, we reproduce the observed data in both near and far field. The agreement between the simulated and observed triggering rates in the far field -- in the absense of farfield tuning of the model -- is an important confirmation of the hypothesis that **the number of triggered earthquakes scales linearly with strain** in both the near and farfield.